Dielectronic recombination of lithiumlike Ni^{25+} ions: High-resolution rate coefficients and influence of external crossed electric and magnetic fields

S. Schippers, T. Bartsch, C. Brandau, and A. Müller
Institut für Kernphysik, Universität Giessen, 35392 Giessen, Germany

G. Gwinner, G. Wissler, M. Beutelspacher, M. Grieser, and A. Wolf
Max-Planck-Institut für Kernphysik and Physikalisches Institut der Universität Heidelberg, 69117 Heidelberg, Germany

R. A. Phaneuf
Department of Physics, University of Nevada, Reno, Nevada 89557
(Received 16 February 2000; published 17 July 2000)

Absolute dielectronic recombination (DR) rates for lithiumlike $Ni^{25+}(1s^22s)$ ions were measured at high-energy resolution at the Heidelberg heavy-ion storage ring TSR. We studied the center-of-mass energy range 0–130 eV which covers all $\Delta n=0$ core excitations. The influence of external crossed electric (0–300 V/cm) and magnetic (41.8–80.1 mT) fields was investigated. For the measurement at near-zero electric field, resonance energies and strengths are given for Rydberg levels up to $n=32$; also Maxwellian plasma rate coefficients for the $\Delta n=0$ DR at electron temperatures between 0.5 and 200 eV are provided. For increasing electric-field strength we find that for both the $2p_{1/2}$ and $2p_{3/2}$ series of $Ni^{24+}(1s^22p_jnl)$ Rydberg resonances with $n>30$, the DR rate coefficient increases approximately linearly by up to a factor of 1.5. The relative increase due to the applied electric field for Ni^{25+} is remarkably lower than that found in previous measurements with lighter isoelectronic Si^{11+}, Cl^{14+}, and Ti^{19+} ions [T. Bartsch *et al.*, Phys. Rev. Lett. **79**, 2233 (1997); **82**, 3779 (1999); J. Phys. B **33**, L453 (2000)], and in contrast to the results for lighter ions no clear dependence of the electric-field enhancement on the magnetic-field strength is found. The Maxwellian plasma rate coefficients for $\Delta n=0$ DR of Ni^{25+} are enhanced by at most 11% in the presence of the strongest experimentally applied fields.

PACS number(s): 34.80.Lx, 32.60.+i, 36.20.Kd, 52.20.−j

I. INTRODUCTION

Dielectronic recombination (DR) is an electron-ion collision process which is well known to be important in astrophysical and fusion plasmas [1,2]. In DR the initially free electron is transferred to a bound state of the ion via a doubly excited intermediate state which is formed by an excitation of the core and a simultaneous attachment of the incident electron. This two-step process

$$e^- + A^{q+} \rightarrow [A^{(q-1)+}]^{**} \rightarrow A^{(q-1)+} + h\nu \qquad (1)$$

involves dielectronic capture (time-inverse Auger process) as the first step, with a subsequent stabilization of the lowered charge state by radiative decay to a state below the ionization limit. This second step competes with autoionization, which would transfer the ion back into its initial charge state q, with the net effect being resonant elastic or inelastic electron scattering. Another recombination process, which in contrast to DR is nonresonant, is radiative recombination (RR),

$$e^- + A^{q+} \rightarrow A^{(q-1)+} + h\nu, \qquad (2)$$

where the initially free electron is transferred to a bound state of the ion, and a photon is emitted simultaneously. The cross section for RR diverges at zero electron energy, and decreases rapidly toward higher energies. In the present investigation we regard RR as a continuous background on top of which DR resonances are emerging.

In the case of narrow nonoverlapping DR resonances, the DR cross section due to an intermediate state labeled d can be well approximated by [3]

$$\sigma_d(E_{\mathrm{cm}}) = \overline{\sigma}_d L_d(E_{\mathrm{cm}}), \qquad (3)$$

with the electron-ion center-of-mass (c. m.) frame energy E_{cm}, the Lorentzian line shape $L_d(E)$ normalized to $\int L_d(E)dE=1$, and the resonance strength

$$\overline{\sigma}_d = 4.95\times 10^{-30}\,\mathrm{cm^2\,eV^2\,s} \times \frac{1}{E_d}\frac{g_d}{2g_i}\frac{A_a(d\rightarrow i)\sum_f A_r(d\rightarrow f)}{\sum_k A_a(d\rightarrow k)+\sum_{f'} A_r(d\rightarrow f')}, \qquad (4)$$

where E_d is the resonance energy, g_i and g_d are the statistical weights of the initial ionic core i and the doubly excited intermediate state d, and $A_a(d\rightarrow i)$ and $A_r(d\rightarrow f)$ denote the rates for an autoionizing transition from d to i and the rate for a radiative transition from d to states f below the first ionization limit, respectively. The summation indices k and f' run over all states which from d can either be reached by autoionization or by radiative transitions, respectively.

It is well known that the cross section for DR via high Rydberg states is enhanced by l mixing in external electric fields [4]. Recently the sensitivity of the electric-field-

 ©2000 The American Physical Society

enhanced DR cross section to additional magnetic fields was predicted [5–7] and experimentally verified [8–10]. This latest progress was summarized by Schippers *et al.* [11].

The aim of the present investigation with Li-like Ni^{25+} is to extend the previous studies of dielectronic recombination in the presence of external fields (DRF) with lighter Li-like Si^{11+} [12], Cl^{14+} [8], and Ti^{19+} [10] ions to an ion with even higher nuclear charge Z. Because of the strong scaling of radiative rates with Z, it is expected that with higher Z fewer l states of a given Rydberg n level take part in DR, and therefore the sensitivity to l mixing in an electric field decreases [13]. Results of Griffin and Pindzola [14], who calculated decreasing DR rate enhancements for increasing charge states of iron ions, pointed in the same direction. Another aspect of going to higher Z is that even high-lying $2p_j nl$ Rydberg resonances are more separated in energy, and are therefore easier to resolve. As with Ti^{19+} ions [10], we are able to study DRF separately for both the $2p_{1/2}nl$ and $2p_{3/2}nl$ series of Rydberg resonances when using Ni^{25+} ions.

II. EXPERIMENT

The measurements were performed at the heavy-ion storage ring TSR [15] of the Max-Planck-Institut für Kernphysik in Heidelberg. For a general account of experimental techniques at heavy-ion storage rings, the reader is referred to a paper by Müller and Wolf [16]. Recombination measurements at storage rings were recently reviewed by Müller [17], Schippers [18], and Wolf *et al.* [19]. Detailed descriptions of the experimental procedure for field free DR measurements were given by Kilgus *et al.* [20], and more recently by Lampert *et al.* [21]. Therefore, here we only describe more explicitly experimental aspects pertaining especially to the present investigation.

The $^{58}Ni^{25+}$ ion beam was supplied by the MPI tandem booster facility, and injected into the TSR with an energy of 343 MeV. Using multiturn injection and *e*-cool stacking [22] electrical ion currents of up to 3300 μA were stored in the TSR. At these high ion currents, however, intrabeam scattering heated the ion beam during DR measurements, resulting in a considerable loss of energy resolution. To avoid this and to limit the recombination count rate to below 1 MHz, i.e., to below a count rate where dead time effects are still negligible, we kept ion currents below 1 mA during all DR measurements. In the storage ring the circulating Ni^{25+} ions were merged with the magnetically guided electron beam of the electron cooler. In the present experiment the electron density was 5.4×10^6 cm^{-3} at cooling energy. Generally the electron density varies with the cathode voltage U_c, thereby following a $U_c^{3/2}$ dependence. The distribution of collision velocities in the electron-ion center of mass frame can be described by the anisotropic Maxwellian

$$f(\vec{v},v_{\rm rel})=\frac{m_e}{2\pi k_B T_\perp}\exp\left(-\frac{m_e v_\perp^2}{2k_B T_\perp}\right)\times\left[\frac{m_e}{2\pi k_B T_{||}}\right]^{1/2}\exp\left(-\frac{m_e(v_{||}-v_{\rm rel})^2}{2k_B T_{||}}\right) \quad (5)$$

characterized by the longitudinal and transverse temperatures $T_{||}$ and $T_\perp$. In Eq. (5), m_e is the electron mass, k_B is the Boltzmann constant, and $v_{\rm rel}$ is the detuning of the average longitudinal electron velocity from that at cooling, which determines the relative energy $E_{\rm rel}\approx m_e v_{\rm rel}^2/2$ between the electron and the ion beam. The longitudinal temperature, inferred from the experimental resolution for relative energies $E_{\rm rel}\gg k_B T_\perp$, was $k_B T_{||}\approx 0.25$ meV. It implies an energy resolution given by ΔE (full width at half maximum) equal to $4\sqrt{\ln(2) k_B T_{||} E_{\rm rel}}$ [20]. The longitudinal velocity spread of the stored ion beam yields a considerable contribution to this temperature, while the velocity spread of the electron beam alone, after acceleration, is estimated to be <0.1 meV. In the transverse direction the electron beam was adiabatically expanded [23] from a diameter $d_c\approx 9.5$ mm at the cathode to a diameter $d_e=29.5$ mm in the interaction region; the reduction of its transverse velocity spread by this expansion determines the low value of the transverse temperature of $k_B T_\perp \approx 10$ meV.

Before starting a measurement, the ion beam was cooled for 5 s, until the beam profiles reached their equilibrium widths. This can be monitored online by employing beam profile monitors based on residual gas ionization [24]. The cooled ion beam had a diameter $d_i\approx 2$ mm. During the measurement the electron cooler voltage was stepped through a preset range of values different from the cooling voltage, thus introducing nonzero mean relative velocities between ions and electrons. Recombined Ni^{24+} ions were counted as a function of the cooler voltage with a CsI-scintillation detector [25] located behind the first dipole magnet downstream of the electron cooler. The dipole magnet bends the circulating Ni^{25+} ion beam onto a closed orbit, and separates the recombined Ni^{24+} ions from that orbit.

Two different measurement schemes were applied for the measurement of (i) a high-resolution ''field-free'' DR spectrum (residual stray electric fields $\leqslant 5$ V/cm), and (ii) DRF spectra with motional electric fields ranging up to 300 V/cm. In view of the result of Huber and Bottcher [26], who calculated that purely magnetic fields below 5 T do not influence DR, the use of the term field-free seems justified in case (i) even with the magnetic guiding field (up to 80 mT) still present in the electron cooler.

A. Procedure for a field-free high-resolution measurement

In between two measurement steps for different values of $E_{\rm rel}$, the cooler voltage was first set back to the cooling value in order to maintain the ion beam quality and then set to a reference value which is chosen to lead to a relative velocity where the electron-ion recombination signal is very small, being favorably due only to a negligible RR contribution (the reference relative energy $E_{\rm ref}$). Under this condition the recombination rate measured at the reference point monitors the background signal due to electron capture from residual gas molecules. Choosing short-time intervals of the order of only 10 ms for dwelling on the measurement, cooling and reference voltages ensured that the experimental environment did not change significantly between the signal and the background measurements. An additional interval of 1.5 ms

after each change of the cooler voltage allowed the power supplies to reach the preset values before data taking was started.

The electron-ion recombination coefficient

$$\alpha(E_{\rm rel}) = \int d^3\vec{v}\, \sigma(v) v f(\vec{v}, v_{\rm rel}) \tag{6}$$

is obtained from the background corrected recombination count rate $R(E_{\rm rel}) - R(E_{\rm ref})$, the detection efficiency η, the electron density n_e, the number of stored ions N_i, the nominal length $L = 1.5$ m of the interaction zone, and the ring circumference $C = 55.4$ m, using the relation

$$\alpha(E_{\rm rel}) = \frac{R(E_{\rm rel}) - R(E_{\rm ref})}{\gamma_i^{-2}\, \eta\, n_e(E_{\rm rel}) N_i L/C} + \alpha(E_{\rm ref}) \frac{n_e(E_{\rm ref})}{n_e(E_{\rm rel})}, \tag{7}$$

where $\gamma_i = 1 + E_i/(m_i c^2)$ is the relativistic Lorentz factor for the transformation between the c. m. and the laboratory frames, where the ions of mass m_i have the kinetic energy E_i. The detection efficiency of the CsI-scintillation detector [25] used to detect the recombined ions is very close to unity for count rates up to 2.5 MHz. The second term in Eq. (7) is to be added in case of a non-negligible electron-ion recombination rate at the reference energy. We insert the theoretical RR rate at $E_{\rm ref} = 131.5$ eV, which we have calculated to be $\alpha(E_{\rm ref}) = 1.39 \times 10^{-11}$ cm^3/s using a semiclassical formula for the radiative recombination cross section [27]

$$\sigma_{RR}(E_{\rm rel}) = 2.1 \times 10^{-22}\ \text{cm}^2 \times \sum_{n_{\rm min}}^{n_{\rm cut}} k_n t_n \frac{q^4 \mathcal{R}^2}{n E_{\rm rel} (q^2 \mathcal{R} + n^2 E_{\rm rel})}, \tag{8}$$

with $\mathcal{R}$ denoting the Rydberg constant and k_n being correction factors given by Andersen and Bolko [28]. This expression for recombination on bare nuclei is used to approximately describe RR on a lithiumlike core by introducing the lowest quantum number $n_{\rm min} = 2$ and weight factors t_n accounting for partial occupation of n shells. In our calculation we use $t_2 = 7/8$ and $t_n = 1$ for $n > 2$. For the maximum (cutoff) quantum number we use $n_{\rm cut} = 150$, as explained below.

After the generation of a recombination spectrum from the experimental data via Eq. (7), a correction procedure accounting for nonperfect beam overlap in the merging sections of the cooler is applied [21], which in our case only slightly redistributes the DR resonance strengths, resulting in DR peaks narrower and taller by small amounts. The systematic uncertainty in the absolute recombination rate coefficient is due to the ion and electron current determination, the corrections accounting for the merging and demerging sections of the electron and ion beams, and the detection efficiency. It is estimated to be $\pm 15\%$ of the measured recombination rate coefficient [21]. The statistical uncertainty of the results presented below amounts to less than 1% of the rate coefficient maximum.

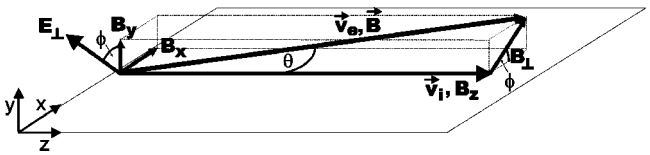

FIG. 1. Sketch of the electric- and magnetic-field configurations used in DRF measurements. The ion beam is aligned along B_z. The motional electric field is $E_\perp = v_i B_\perp = v_i \sqrt{B_x^2 + B_y^2}$, with the ion velocity v_i in the z direction. The azimuthal angle ϕ denotes the direction of $E_\perp$ in the x-y plane. The electron beam with the average velocity $\vec{v}_e$ is aligned along the resulting $\vec{B}$ vector which is inclined by the angle θ with respect to B_z.

B. Procedure for DRF measurements

The geometry of the magnetic and electric fields present in the merging section of the electron cooler is sketched in Fig. 1. We choose the z axis to be defined by the ion-beam direction. The magnetic guiding field $\vec{B}$ defines the electron-beam direction. The field strength B is limited towards both low and high values. Only fields $B > 25$ mT guarantee a reliable operation of the electron cooler. The maximum tolerable current through the generating coils limits B to at most 80 mT. Correction coils allow the steering of the electron beam in the x-y plane. In the first place these are used to minimize the transverse field components B_x and B_y with respect to the ion beam, such that the two beams are collinear and centered to each other. The collinearity is inferred indirectly from beam profile measurements of the cooled ion beam [24] with an accuracy of ~ 0.2 mrad; i.e., the transverse magnetic-field components caused by imperfections in the beam alignment amounts at most to $2 \times 10^{-4} B$. Residual fields which may vary in size and direction along the overlap length, are also expected to be of this magnitude. Since the settings of the various steering magnets result from a rather tedious beam optimization process, they are not exactly reproduced after each optimization procedure that is required, e.g., after a change of the magnetic guiding field B_z. This means that the residual transverse magnetic fields for the collinear geometry may also slightly vary from one set of cooler settings to another. All uncertainties in the transverse magnetic field translate into an uncertainty in the motional electric field of less than ± 10 V/cm in our present experiment.

In DRF measurements we offset the current through the correction coils to generate additional magnetic-field components B_x and B_y. Their influence on the stored ion beam is negligible, i.e., the ion beam is still traveling with velocity $v_{\rm i}$ in the z direction. However, in the frame of the ion beam the magnetic-field components B_x and B_y generate a motional electric field $E_\perp = \sqrt{E_y^2 + E_x^2} = v_{\rm i} \sqrt{B_x^2 + B_y^2}$ in the x-y plane rotated out of the y direction by the azimuthal angle $\phi = \arctan(B_y/B_x) = \arctan(E_x/E_y)$, i.e., $E_\perp = E_y$ for $\phi = 0$. The electrons (due to their much lower mass) follow the resulting magnetic-field vector $\vec{B}$ which now crosses the ion beam at the angle $\theta = \arctan(\sqrt{B_x^2 + B_y^2}/B_z)$. Two consequences are to be dealt with: (i) The ion beam now probes different portions of the space-charge well of the electron beam. This reduces the energy resolution. In order to minimize this effect we

used a rather small electron density of only 5.4×10^6 cm^{-3} at cooling, i.e., one order of magnitude smaller than in the Si^{11+} experiment of Bartsch *et al.* [12]. (ii) The angle θ between the electron beam and ion beam explicitly enters the formula for the transformation from the laboratory system to the c. m. system, which is easily derived from the conservation of 4 momentum. It reads

$$E_{\rm rel}=m_ic^2(1+\mu)\left[\sqrt{1+\frac{2\mu}{(1+\mu)^2}(\Gamma-1)}-1\right], \quad (9)$$

with the mass ratio $\mu=m_e/m_i$,

$$\Gamma=\gamma_i\gamma_e-\sqrt{(\gamma_i^2-1)(\gamma_e^2-1)}\cos\theta, \quad (10)$$

and $\gamma_e=1+E_e/m_ec^2$; E_e denotes the electron laboratory energy. It is obvious that the cooling condition $E_{\rm rel}=0$ can only be reached for $\gamma_i=\gamma_e$ and $\theta=0$, i.e., for $\Gamma=1$. In regular field-free measurements a scheme of intermittent cooling is used during data taking, i.e. after each measured energy a cooling interval ($E_{\rm rel}=0$) is inserted. For DRF measurements this would require a rapid switching from $\theta\neq0$ to cooling with $\theta=0$. It turned out that such a procedure heavily distorts the electron beam, mainly because of the slow response of the power supplies controlling the steering coils. Under such conditions useful measurements could not be performed. Therefore, we omitted the intermittent cooling and reference measurement intervals, thereby losing resolution. After each injection into the ring and an appropriate cooling time, the correction coils were set to produce a defined $E_\perp$, and the cathode voltage was ramped very quickly through a preset range with a dwell time of only 1 ms per measurement point. In such a manner a spectrum for one $E_\perp$ setting was collected within only 4 s. After termination of the voltage ramp the correction coils were set back to $\theta=0$, and the whole cycle started again with the injection of ions into the ring. In subsequent cycles a range of typically 30 preset $E_\perp$ values was scanned. Each spectrum was measured as many times as needed for reaching a satisfying level of statistical errors. This whole procedure was repeated for different settings of the guiding field strength B_z.

In order to compare only contributions from DR to the measured spectra, we subtracted an empirical background function $\alpha_{\rm BG}(E_{\rm rel})=a_0+a_1E_{\rm rel}+a_2/(1+a_3E_{\rm rel}+a_4E_{\rm rel}^2)$, with the coefficients a_i determined by fitting $\alpha_{\rm BG}(E_{\rm rel})$ to those parts of the spectrum which do not exhibit DR resonances. One should note that a proper calculation of the RR rate coefficient is hampered by the fact that for $\theta\neq0$ the electron velocity distribution probed by the ion beam cannot be described by Eq. (5).

III. RESULTS AND DISCUSSION

A. Recombination at zero electric field

1. DR cross section

For the $\Delta n=0$ DR channels of Li-like Ni^{25+}, i.e., for DR involving excitations which do not change the main quantum number of any electron in the $1s^22s$ core, Eq. (1) reads, more explicitly,

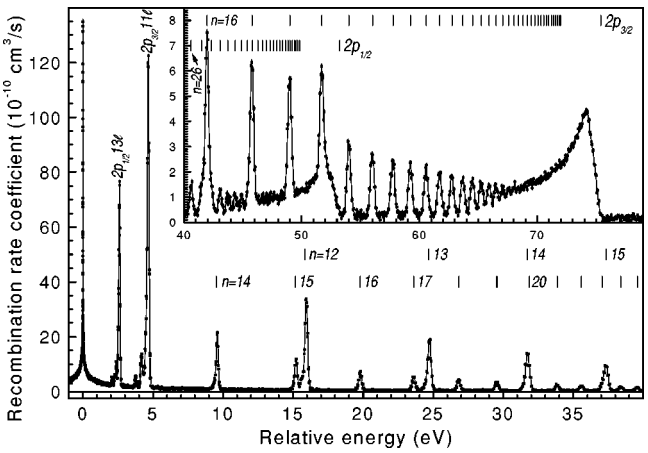

FIG. 2. Absolute recombination rate coefficient measured for 340-MeV Ni^{25+} ions. The sharp peak at zero relative energy is due to RR. Energetic positions of the $2p_{1/2}nl$ and $2p_{3/2}nl$ resonances according to the Rydberg formula are indicated.

$$\begin{aligned} e^- + {\rm Ni}^{25+}(1s^22s_{1/2}) &\rightarrow {\rm Ni}^{24+}(1s^22p_jnl) \\ &\rightarrow \begin{cases} {\rm Ni}^{24+}(1s^22s_{1/2}nl)+h\nu & \text{(type I)} \\ {\rm Ni}^{24+}(1s^22p_jn'l')+h\nu' & \text{(type II)}. \end{cases} \end{aligned} \quad (11)$$

The lowest Rydberg states which are energetically allowed are $n=13$ and 11 for $2s_{1/2}\rightarrow2p_{1/2}$ and $2s_{1/2}\rightarrow2p_{3/2}$ core excitations, respectively.

The $Ni^{25+}(1s^22s_{1/2})$ recombination spectrum has been measured for $0\leqslant|E_{\rm rel}|\leqslant131.5$ eV. The result is shown in Fig. 2. At $E_{\rm rel}=0$, a sharp rise of the recombination rate due to RR is observed. At higher energies DR resonances due to $\Delta n=0$ $2s_{1/2}\rightarrow2p_j$ transitions occur. Individual $2p_jnl$ resonances are resolved for $n\leqslant32$. Their resonance strengths have been extracted from the measured spectrum by first subtracting the theoretical recombination rate coefficient due to RR (cf. Sec. II A), where the c. m. velocity spread can be neglected since $E_{\rm rel}$ is very large compared to $kT_\perp$ and $kT_\parallel$. In principle the resulting rate coefficient should be zero at off-resonance energies. However, we find that, probably due to our approximate treatment of RR [cf. Eq. (8)], small nonzero rate coefficients remain after subtraction of the calculated RR rate coefficient. These are removed by further subtracting a smooth background before the observed DR resonance structures are fitted by Gaussians. (Details of the observed smooth RR rate were not further investigated in the present work.) The resulting values for resonance positions and strengths are listed in Table I. The $2p_{1/2}13l$ and $2p_{3/2}11l$ resonances at about 2.5 and 4.5 eV, respectively, exhibit a splitting due to the interaction of the nl Rydberg electron with the $1s^22p_j$ core. For higher n resonances this splitting decreases, and cannot be observed because of the finite experimental energy spread which increases as $\sqrt{E_{\rm rel}}$. The $2p_j$ Rydberg series limits E_∞ are obtained from a fit of the resonance positions E_n with $n\geqslant16$ to the Rydberg formula,

TABLE I. Strengths of the individually resolved $2p_j nl$ resonances as obtained from fits of Gaussians to the experimentally observed resonance structures. The errors given are statistical only (one standard deviation). Systematic uncertainties amount to less than $\pm 15\%$ for the resonance strengths, and less than 0.6% for the resonance positions.

Resonance position E_d (eV)	Resonance strength $\overline{\sigma_d}$ (10^{-19} eV cm^2)	Designation
2.079 ± 0.002	2.42 ± 0.12	$2p_{1/2}13s$
2.267 ± 0.003	3.25 ± 0.22	$2p_{1/2}13p$
2.383 ± 0.001	9.53 ± 0.26	$2p_{1/2}13d$
2.625 ± 0.003	94.2 ± 5.7	$2p_{1/2}13l(l>2)$
9.590 ± 0.003	22.7 ± 0.71	$2p_{1/2}14l$
15.21 ± 0.001	11.1 ± 0.12	$2p_{1/2}15l$
19.81 ± 0.002	6.78 ± 0.083	$2p_{1/2}16l$
23.63 ± 0.002	4.85 ± 0.077	$2p_{1/2}17l$
26.83 ± 0.003	3.71 ± 0.072	$2p_{1/2}18l$
29.54 ± 0.003	2.77 ± 0.057	$2p_{1/2}19l$
33.84 ± 0.004	1.98 ± 0.046	$2p_{1/2}21l$
35.57 ± 0.004	1.72 ± 0.045	$2p_{1/2}22l$
38.40 ± 0.005	1.32 ± 0.044	$2p_{1/2}24l$
39.55 ± 0.009	1.13 ± 0.065	$2p_{1/2}25l$
40.63 ± 0.006	1.02 ± 0.040	$2p_{1/2}26l$
41.53 ± 0.024	1.13 ± 0.10	$2p_{1/2}27l$
42.35 ± 0.023	0.935 ± 0.14	$2p_{1/2}28l$
43.09 ± 0.008	0.857 ± 0.042	$2p_{1/2}29l$
43.75 ± 0.012	0.739 ± 0.051	$2p_{1/2}30l$
44.35 ± 0.014	0.744 ± 0.063	$2p_{1/2}31l$
44.91 ± 0.013	0.727 ± 0.063	$2p_{1/2}32l$
3.777 ± 0.002	4.71 ± 0.13	$2p_{3/2}11s$
4.190 ± 0.001	17.9 ± 0.17	$2p_{3/2}11p$
4.673 ± 0.001	163.3 ± 2.1	$2p_{3/2}11l(l>1)$
15.96 ± 0.001	40.4 ± 0.61	$2p_{3/2}12l$
24.73 ± 0.002	20.04 ± 0.66	$2p_{3/2}13l$
31.74 ± 0.001	15.2 ± 0.14	$2p_{1/2}20l, 2p_{3/2}14l$
37.34 ± 0.004	10.33 ± 0.30	$2p_{1/2}23l, 2p_{3/2}15l$
41.95 ± 0.003	6.61 ± 0.20	$2p_{3/2}16l$
45.77 ± 0.002	5.38 ± 0.047	$2p_{3/2}17l$
48.97 ± 0.002	4.45 ± 0.045	$2p_{3/2}18l$
51.70 ± 0.003	4.01 ± 0.17	$2p_{3/2}19l$
54.00 ± 0.003	2.68 ± 0.039	$2p_{3/2}20l$
55.99 ± 0.003	2.32 ± 0.038	$2p_{3/2}21l$
57.73 ± 0.004	2.02 ± 0.038	$2p_{3/2}22l$
59.22 ± 0.004	1.88 ± 0.037	$2p_{3/2}23l$
60.56 ± 0.004	1.75 ± 0.035	$2p_{3/2}24l$
61.72 ± 0.005	1.61 ± 0.036	$2p_{3/2}25l$
62.75 ± 0.005	1.46 ± 0.034	$2p_{3/2}26l$
63.68 ± 0.005	1.40 ± 0.035	$2p_{3/2}27l$
64.49 ± 0.005	1.30 ± 0.037	$2p_{3/2}28l$
65.27 ± 0.008	1.23 ± 0.040	$2p_{3/2}29l$
65.93 ± 0.009	1.16 ± 0.040	$2p_{3/2}30l$
66.52 ± 0.01	1.11 ± 0.041	$2p_{3/2}31l$

TABLE II. Parameters obtained from fits of DR resonance positions and strengths. The series limits E_∞, and their uncertainties and quantum defects δ, result from a fit of the experimental resonance positions to the Rydberg formula [Eq. (12)]. The total experimental uncertainty of E_∞ is of the order of ± 0.5 eV. The spectroscopic values listed for comparison are taken from Ref. [29]. In the fit of Eq. (13) to the measured DR resonance strengths, the core radiative rates $A_r^{(\mathrm{I})}$ and the Auger rates A_a (as listed) have been taken from atomic structure calculations [32]. S_0 and $A_r^{(\mathrm{II})}$ result from the fit. $l_{\max}$ has been calculated from S_0.

Series	$2p_{1/2}$	$2p_{3/2}$
E_∞ (eV), spectroscopic	52.95	74.96
E_∞ (eV), this experiment	53.19 ± 0.01	75.34 ± 0.01
δ	0.031 ± 0.005	0.030 ± 0.001
A_a (10^{15} s^{-1})	0.4	1.2
$A_r^{(\mathrm{I})}$ (10^9 s^{-1})	2.0	5.8
$A_r^{(\mathrm{II})}$ (10^{13} s^{-1})	4.1 ± 0.6	6.7 ± 0.5
S_0 (10^{-27} eV^2 cm^2 s)	1.19 ± 0.09	1.12 ± 0.03
$l_{\max}$	14.5 ± 0.6	9.5 ± 0.2

$$E_n = E_\infty - \mathcal{R}\left(\frac{q}{n-\delta}\right)^2, \tag{12}$$

with the quantum defect δ as a second fit parameter. The fit results are listed in Table II, where spectroscopic values [29] for the series limits are also given. Our values agree with the spectroscopic values within 0.6%, i.e., within the experimental uncertainty of the energy scale [20]. The result that the fitted quantum defects are almost zero reflects the fact that the interaction between the core electrons and the Rydberg electron is weak.

The measured DR rate decreases already below the $2p_{1/2}$ and $2p_{3/2}$ series limits, as obtained from the fit to the peak positions (cf. Fig. 2). This discrepancy results from field ionization of high Rydberg states with $n>n_f\approx(3.2\times10^8\mathrm{V/cm}\,q^3/E_{\mathrm{dip}})^{1/4}$ in the charge-analyzing dipole magnet (see Sec. II) with magnetic-field strength $B_{\mathrm{dip}}=0.71$ T, where the moving ion experiences the motional electric field $E_{\mathrm{dip}}=v_i B_{\mathrm{dip}}$ (n_f is the classical field ionization limit). A more realistic value for the cutoff has to account for Stark splitting and tunneling effects. In Ref. [13] an approximate value $n_{\mathrm{cut}}\approx(7.3\times10^8\mathrm{V/cm}\,q^3/E_{\mathrm{dip}})^{1/4}$ was found. For the calculation of the actual cutoff quantum number n_{cut} relevant in this experiment, one has to take into account that on the way from the cooler to the dipole magnet states with $n>n_f$ may radiatively decay to states below n_f. An approximate calculation of this effect [30] yields $n_{\mathrm{cut}}=150$ for the present case.

An estimate of the DR line strength escaping detection because of field ionization can be made by extrapolating the measured DR line strength to $n=\infty$, employing the n^{-3} scaling of the autoionization and the type-II [cf. Eq. (11)] radiative rates [31]. For autoionization rates we make the ansatz $A_a(nl)=A_a/n^3$ for $0\leqslant l\leqslant l_{\max}$ and $A_a(nl)=0$ for $l_{\max}<l<n$. Rates for the sum of type-I and -II radiative transitions we represent as $A_r(nl)=A_r^{(\mathrm{I})}+A_r^{(\mathrm{II})}/n^3$. The same represen-

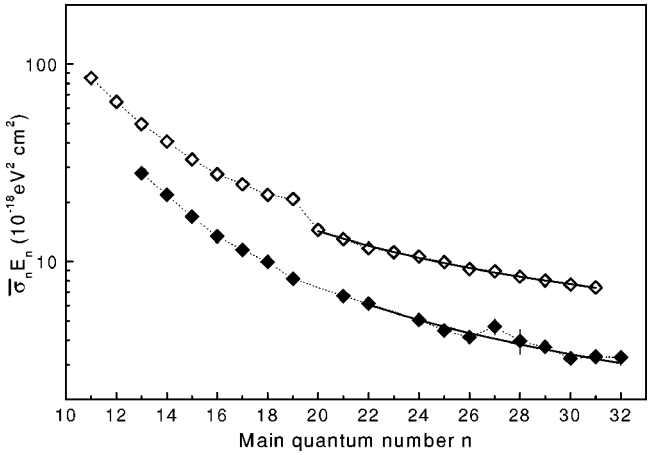

FIG. 3. Product of strength and resonance energy of the $2p_j nl$ DR resonances for $j=1/2$ (closed symbols) and $j=3/2$ (open symbols), as extracted from the experimental recombination spectrum. Statistical error bars are mostly smaller than the symbol size. The strengths of the $2p_{3/2}14l$ and $2p_{3/2}15l$ resonances have been obtained by subtracting interpolated values for the $2p_{1/2}20l$ and $2p_{1/2}23l$ resonance strengths from the measured peak areas at 31.7 and 37.3 eV, respectively. The thick full curves represent fits according to Eq. (13) with the fit parameters listed in Table II.

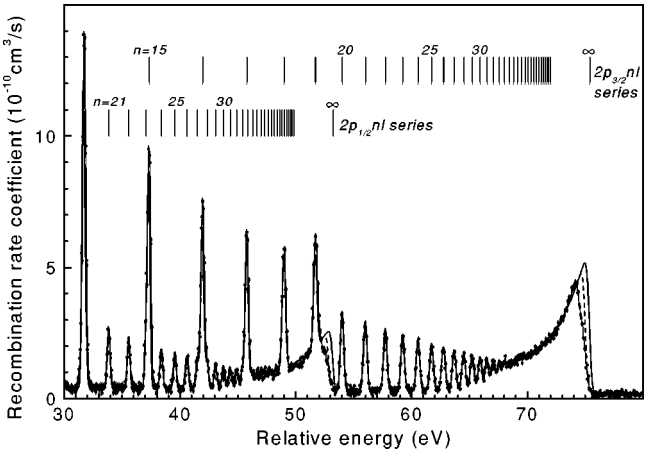

FIG. 4. Comparison between measured (closed symbols) and extrapolated recombination spectra (see text). The extrapolations extend to $n=150$ (dashed line) and $n=500$ (full line), where convergence is achieved.

tations of the relevant rates were already used by Kilgus *et al.* [20] in a recombination study of isoelectronic Cu^{26+} ions. After summation over all l substates, Eq. (4) simplifies to

$$\overline{\sigma_n E_n} = S_0 \frac{A_a [A_r^{(\mathrm{I})} + n^{-3} A_r^{(\mathrm{II})}]}{A_a + n^3 A_r^{(\mathrm{I})} + A_r^{(\mathrm{II})}}, \tag{13}$$

with $S_0 = 2.475(2j_c+1)(l_{\max}+1)^2 \times 10^{-30}$ cm^2 eV^{2}s. For the statistical weights in Eq. (4), we have used $g_i = 2$ and $g_d = 2(2l+1)(2j_c+1)$. Here, j_c is the total angular momentum quantum number of the core excited state, i.e., $j_c = 1/2$ and 3/2 in the present case. The first step of the extrapolation procedure consists of adjusting the model parameters such that Eq. (13) fits the measured DR line strengths. Here the values for $A_r^{(\mathrm{I})}$ have been taken from atomic structure calculations [32] while S_0, A_a, and $A_r^{(\mathrm{II})}$ were allowed to vary during the fit. It turned out that the fit is not very sensitive to large variations of the Auger rates A_a. In this situation we also kept the Auger rates fixed at values which have been inferred from atomic structure calculations, and which are meant to be order of magnitude estimates only. In Fig. 3 we plot the measured and fitted resonance strengths (multiplied by the resonance energy) as a function of the main quantum number. The actual parameters used for drawing the fit curves are listed in Table II. The fit has been restricted to $n \geqslant 20$ for both the $2p_{1/2}$ and $2p_{3/2}$ series, because additional Coster-Kronig decay channels $2p_{3/2}nl \rightarrow 2p_{1/2}\epsilon l'$ open up when E_n crosses the $2p_{1/2}$ series limit. A corresponding discontinuous decrease of the $2p_{3/2}nl$ DR resonance strength can be clearly discerned in Fig. 3. Since the additional autoionizing channels are included for the $2p_{3/2}nl$ series of resonances but not for the $2p_{1/2}nl$ series, A_a for the $2p_{3/2}nl$ series is more than a factor of 2 higher than A_a for the $2p_{1/2}nl$ series. A factor of 2 would just correspond to the ratio of statistical weights.

Inserting the fit parameters listed in Table II into Eqs. (12) and (13) now allows an extrapolation of the DR resonance positions and strengths, respectively, to be obtained for arbitrarily high n. In order to check the quality of the extrapolation we have convoluted the extrapolated DR cross section with the experimental electron energy distribution using the electron-beam temperatures $k_B T_{||} = 0.25$ meV and $k_B T_{\perp} = 10$ meV. After adding the semiclassically calculated RR rate coefficient—as described above—the resulting extrapolated DR+RR recombination rate coefficient is plotted in Fig. 4 together with the experimental one. Despite the very simple model assumptions, the calculated recombination rate also agrees with the measured one over the energy intervals covered by the $2p_j nl$ resonances with $n > 31$, which are not resolved individually and therefore have not been used for the fits. Deviations from the $Ni^{24+}(1s^2 2p_{3/2}nl)$ resonances with $n \leqslant 19$ stem from the fact that for these resonances the Coster-Kronig decay channels to $Ni^{25+}(1s^2 2p_{1/2})$ are closed, whereas the fit has been made to resonances where they are open. At energies close to the series limits, slight deviations from the model rate occur even when the expected value of $n_{\mathrm{cut}} = 150$ is inserted into the model (the dashed line in Fig. 4). The origin of this discrepancy probably has to be searched for in the approximations made in both the field ionization model and in the model rate descriptions, in particluar regarding the dependence of the angular momentum l, which may be affected by even the small residual electric fields in the interaction region.

2. Maxwellian plasma rate coefficient

The comparison between the measured data and the calculated extrapolation to $n \rightarrow \infty$ (the full line in Fig. 4) suggests that only a minor part of the total Ni^{25+} $\Delta n = 0$ DR resonance strength has not been measured. This enables us to derive the Ni^{25+} DR rate coefficient in a plasma from our

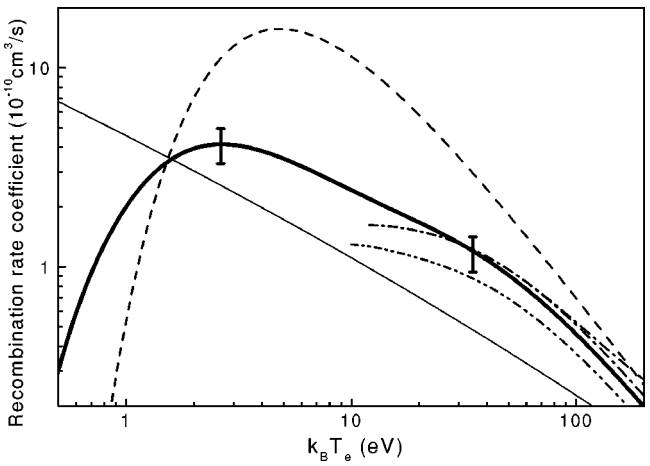

FIG. 5. Ni^{25+} $\Delta n=0$ DR plasma rate coefficient as derived from our measurement (thick full line, estimated error $\pm 20\%$ as indicated). Also shown are theoretical results of Mewe *et al.* [34] (dashed line), Romanik [35] (dash-dotted line), and Teng *et al.* [36] (dash-dot-dotted line). At temperatures $k_B T_e > 100$ eV, two DR rates by Romanik are shown, with the upper one additionally containing $\Delta n=1$ DR contributions. The RR rate coefficient (thin full line) has been calculated from the RR cross section given by Eq. (8), with $q=25$ and $n_{max}=150$.

measurement. To this end the experimental DR rate coefficient is substituted by the extrapolated one at energies ~ 3 eV below the series limits. Compared to using the experimental result without extrapolation, this results in a correction of the plasma rate coefficient of at most 5%. The experimental DR rate coefficient, including the high n extrapolation, is convoluted by an isotropic Maxwellian electron velocity distribution characterized by the electron temperature T_e. The resulting $\Delta n=0$ DR plasma rate coefficient is displayed in Fig. 5 (thick full line). Summing experimental and extrapolation errors, the total uncertainty of the DR rate coefficient in plasmas determined in this work amounts to $\pm 20\%$.

A convenient representation of the plasma DR rate coefficient is provided by the following fit formula:

$$\alpha(T_e) = T_e^{-3/2} \sum_i c_i \exp(-E_i/k_B T_e). \qquad (14)$$

This has the same functional dependence on the plasma electron temperature as the widely used Burgess formula [33], where the coefficients c_i and E_i are related to oscillator strengths and excitation energies, respectively. The results for the fit to the experimental Ni^{25+} $\Delta n=0$ DR rate coefficient in a plasma (the thick full line in Fig. 5) are summarized in Table III. The fitted curve cannot be distinguished from the experimental plasma rate coefficient in a plot, as presented in Fig. 5.

In Fig. 5 we also compare our results with theoretical results for $\Delta n=0$ DR by Mewe *et al.* [34] (dashed line), Romanik [35] (dash-dotted line), and Teng *et al.* [36] (dash-dot-dotted line) who interpolated DR calculations performed by Chen [37] for selected lithiumlike ions. At temperatures $k_B T_e > 1$ eV, the rate of Mewe *et al.*, which is based on the Burgess formula [33], overestimates our experimental result by up to a factor of ~ 5. At lower temperatures the experimental result is underestimated by factors up to 10. Above an electron temperature of 30 eV, Romanik's theoretical result agrees with our $\Delta n=0$ DR rate coefficient to within 15%, which is within the 20% experimental accuracy. In this energy range the interpolation result of Teng *et al.* underestimates the experimental rate coefficient by 20–30 %. It should be noted that neither the calculation of Romanik nor that of Teng *et al.* covers temperatures below 10 eV. When compared with our RR calculation (the thin full line in Fig. 5), our experimental result shows that in the temperature range of 1–10 eV, where Ni^{25+} ions may exist in photoionized plasmas, DR is still significant. The importance of DR in low-temperature plasmas was recently pointed out by Savin *et al.* [38], who measured DR of fluorinelike Fe^{17+} ions. At higher temperatures Romanik's calculation [35] suggests that above 100 eV $\Delta n=1$ DR contributions become significant (the upper dash-dotted line in Fig. 5).

TABLE III. Ni^{25+} $\Delta n=0$ plasma DR rate coefficient fit parameters c_i and E_i according to Eq. (14). The fit to the full line in Fig. 5 is accurate to better than 0.5% for 1.0 eV $\leqslant k_B T_e$. The total uncertainty in the rate coefficient is 20%.

i	c_i (10^{-2} cm^3 s^{-1} K$^{3/2}$)	E_i (eV)
1	0.417	2.91
2	0.683	5.60
3	1.483	19.10
4	3.184	44.54
5	2.928	71.97

B. DRF measurements

Figure 6 shows a series of Ni^{25+} recombination spectra measured in the presence of external electric fields $E_\perp$ rang-

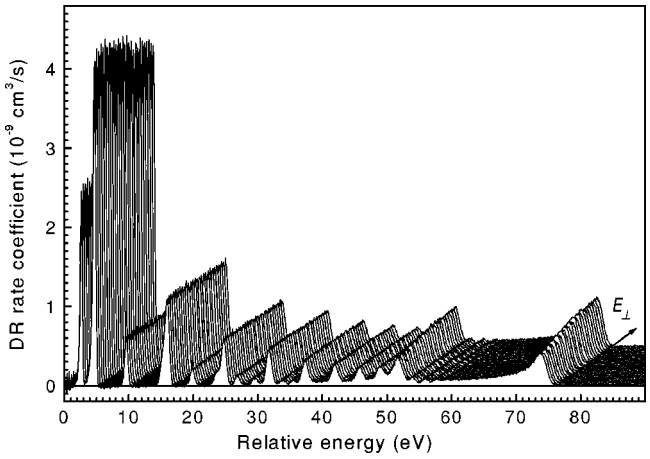

FIG. 6. Ni^{25+} DR spectra for 28 external electric fields $0 \leqslant E_\perp \leqslant 270$ V/cm and $|\cos\phi|=1$. Spectra with $\phi=0°$ and $\phi=180°$ are interleaved. Adjacent spectra differ by $\Delta E_\perp = 10$ V/cm. The magnetic field on the axis of the electron cooler has been $B_z = 80$ mT. The fitted smooth RR contribution has been subtracted.

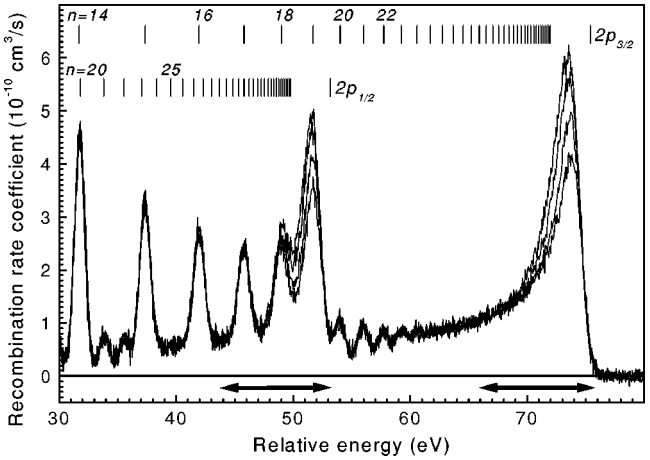

FIG. 7. Ni^{25+} DR spectra for four external electric fields of 0, 110, 190, and 270 V/cm, clearly showing the DR rate enhancement with increasing electric-field strength close to the $2p_{1/2}$ and $2p_{3/2}$ series limits. Ranges for the determination of integrated rate coefficients are indicated by horizontal arrows. The magnetic field on the axis of the electron cooler is $B_z=80$ mT. The fitted smooth RR contribution has been subtracted.

ing from 0 to 270 V/cm. The magnetic field on the axis of the cooler has been set to $B_z=80$ mT. Due to the altered measurement scheme that leaves out the intermittent cooling of the ion beam, the energy resolution is reduced compared to Fig. 2. Now individual $2p_jnl$ DR resonances are resolved only up to $n=21$. Two features in the series of spectra are to be noted. First, the strength of the DR resonances occurring below 47 eV does not depend on $E_\perp$. Second, the strength of the unresolved high-n DR resonances increases with increasing field strength. This can been seen more clearly from the closeup presented in Fig. 7. At energies of more than 10 eV below the $2p_j$ series limits, the different DR spectra lie perfectly on top of each other, whereas at higher energies (i.e. $n>30$) an increase of the DR intensities by up to a factor of 1.5 at $E_\perp=270$ V/cm is observed. The degraded resolution of the DR spectrum does not allow us to resolve n levels in the range of the electric-field enhancement. In order to quantify this DR rate enhancement we consider integrated recombination rates, with the integration intervals chosen as marked in Fig. 7.

The integration intervals 44.0–53.5 and 66.2–76.0 eV include all $2p_jnl$ resonances with $n\geqslant 31$ for $j=1/2$ and 3/2, respectively. In the following we denote the resulting integrals by $I_{1/2}$ and $I_{3/2}$. The energy range 44.0–53.5 eV also contains $2p_{3/2}nl$ resonances with $16\leqslant n\leqslant 19$. These resonances, however, are not affected by the electric-field strengths used in our experiment. Consequently, any change in the magnitude of $I_{1/2}$ as a function of $E_\perp$ we attribute to field effects on $2p_{1/2}nl$ resonances. As a check of the proper normalization of the DR spectra, we additionally monitor the integral $I_0=\int_{2\ \mathrm{eV}}^{18\ \mathrm{eV}}\alpha_{\mathrm{DR}}(E_{\mathrm{rel}})dE_{\mathrm{rel}}$ which comprises the strengths of the $2p_{3/2}11l$, $2p_{3/2}12l$, and $2p_{1/2}nl$ DR resonances with $13\leqslant n\leqslant 15$. Since these low-$n$ resonances are not affected by $E_\perp$, we expect I_0 to be constant. Any deviation of I_0 from a constant value would indicate a reduction of the beam overlap due to too large a tilting angle θ of the

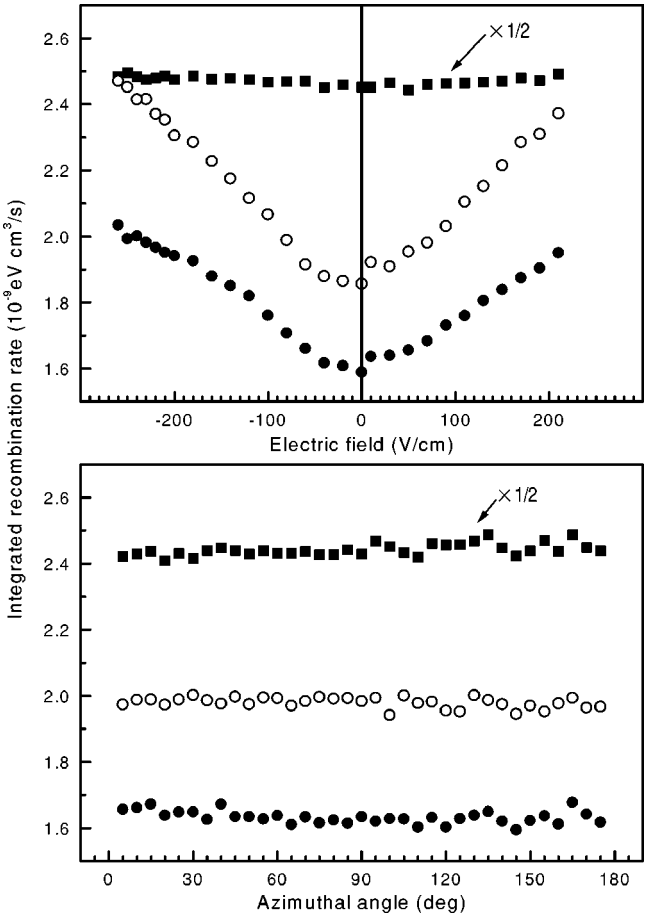

FIG. 8. Integrated recombination rate coefficients I_0 (full squares), $I_{1/2}$ (full circles), and $I_{3/2}$ (open circles) for the integration ranges defined in the text as a function of electric field (upper panel, $\phi=0°$) and of azimuthal angle (lower panel, $E_\perp=100$ V/cm). The magnetic guiding field is 80 mT in both cases.

electron beam. The maximum angle $\theta_{\max}$, to which the overlap of the electron beam with the ion beam is ensured over the full interaction length L, is given by $\tan\theta_{\max}=(d_e-d_i)/L$. With the geometrical values given above, one obtains $\theta_{\max}\approx 1°$. Apart from the highest $E_\perp$ at $\phi=180°$ and at the lowest magnetic guiding field, i.e., at $B_z=41.8$ mT, the condition $\theta<\theta_{\max}$ was always met. This is exemplified in the upper panel of Fig. 8, where I_0, $I_{1/2}$, and $I_{3/2}$ are shown for -270 V/cm$\leqslant E_\perp\leqslant 220$ V/cm. There, a positive (negative) field strength indicates $\phi=0°$ ($\phi=180°$). While $I_{1/2}$ and $I_{3/2}$ clearly exhibit a field effect which is nearly symmetric about $E_\perp=0$ V/cm, I_0 is independent of $E_\perp$.

The fact that the increase of the integrated recombination rate coefficient is independent of the sign of the electric-field vector is expected from the cylindrical symmetry of the merged-beam arrangement in the electron cooler. However, for the entire experimental setup this symmetry is broken by the charge-analyzing dipole magnet with an electric-field vector lying in the bending plane (the x-y plane of the coordinate frame defined in the interaction region). This, in principle, could lead to a redistribution of population between different m substates in the dipole magnet [39] and a resulting field ionization probability depending on the azimuthal

angle ϕ of the motional electric-field vector in the cooler. In order to clarify this question we took a series of DRF spectra with ϕ ranging from 5° to 175°. At the same time the electric and magnetic fields were kept fixed at $E_\perp = 100$ V/cm and $B_z = 80$ mT. A scan around a full circle was prohibited by the limited output of the power supplies used for steering the electron beam in the particular arrangement of this experiment. As shown in the lower panel of Fig. 8, no significant dependence of the integrated recombination rates on the azimuthal angle ϕ was found.

As a measure for the magnitude of the field enhancement, we introduce the field enhancement factor

$$r_j(E_\perp, B_z) = C_j(B_z)\frac{I_j(E_\perp, B_z)}{I_0(E_\perp, B_z)} \tag{15}$$

for $j = 1/2$ or 3/2, and the constant $C_j(B_z)$, chosen such that $r_j(0,B_z) = 1.0$ (see below). Plots of enhancement factors as a function of $E_\perp$ are shown in Fig. 9 for different values of B_z. Since the field effect is independent of the orientation of the electric field in the *x*-*y* plane, data points for $\phi = 0°$ and $\phi = 180°$ are plotted together. The enhancement factor exhibits a linear dependence on the electric field. Exceptions occur for $B_z = 41.8$ mT and $\phi = 180°$ at $E_\perp$ values, where θ becomes maximal, and around $E_\perp = 0$ V/cm. In the former case the complete overlap of the ion beam and the electron beam over the full length of the interaction region is lost. This is indicated by a reduction of I_0, and apparently a consistent normalization cannot be carried out. In the latter case residual electric- and magnetic-field components resulting, e.g., from a nonperfect alignment of the beams, prevent us from reaching $E_\perp = 0$ eV. After excluding all data points with $E_\perp \leqslant 10$ V/cm and those with $\phi = 180°$, $E_\perp \geqslant 200$ V/cm for $B_z = 41.8$ mT, we were able to fit straight lines to the measured field enhancement factors as a function of $E_\perp$. The constants $C_j(B_z)$ in Eq. (15) have been chosen such that the fitted straight lines yield $r_j^{(\mathrm{fit})}(0,B_z) = 1.0$.

As a measure for the electric-field enhancement of the DR rate enhancement, we now consider the slopes

$$s_j(B_z) = \frac{dr_j^{(\mathrm{fit})}(E_\perp, B_z)}{dE_\perp} \tag{16}$$

of the fitted straight lines, which are displayed as a function of the magnetic-field strength in Fig. 10. The error bars correspond to statistical errors only. Systematic uncertainties, e.g., due to residual fields, are difficult to estimate. Nevertheless, their order of magnitude can be judged from the $\approx 10\%$ difference between the two data points at $B_z = 80$ mT which have been measured with different cooler settings.

For all magnetic fields used, the electric-field dependence of the rate enhancement factor is steeper for the $2p_{3/2}nl$ series of Rydberg resonances than that for the $2p_{1/2}nl$ series. This can be understood from the fact that the multiplicity of states—and, consequently, the number of states which can be mixed—is two times higher for $j = 3/2$ than for $j = 1/2$. Following this argument one would expect a ratio of 2 for the respective incremental integrated recombination rates $I_j(E_\perp, B_z) - I_j(0,B_z)$. From our measurements we find lower

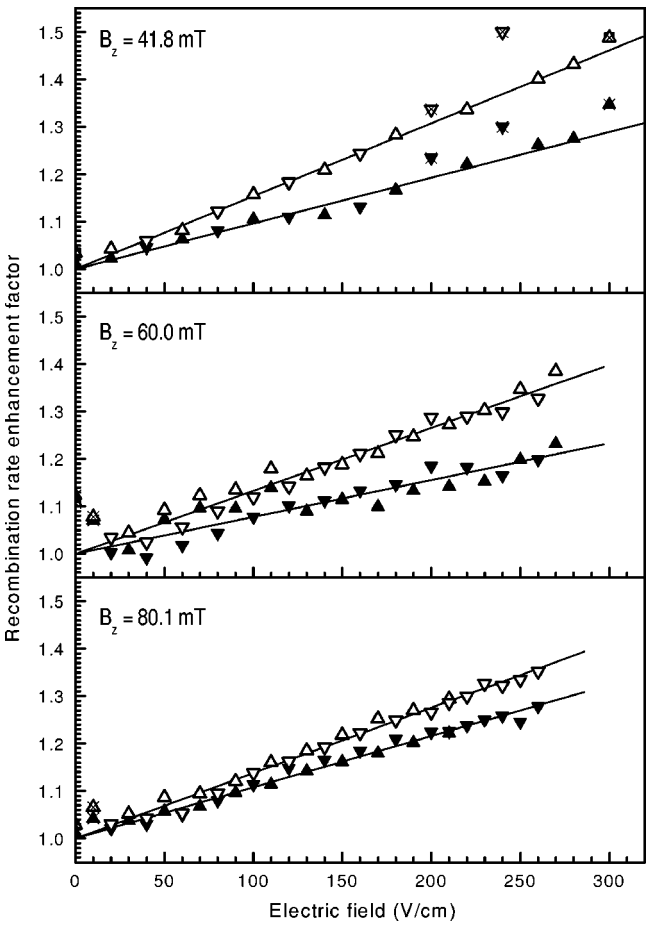

FIG. 9. Recombination rate enhancement factors as a function of electric field $E_\perp$ for three different magnetic fields B_z. The enhancement is larger for the series of $2p_{3/2}nl$ resonances (open symbols), as compared to the $2p_{1/2}nl$ series (closed symbols). Triangles pointing upward (downward) mark data points measured at $\phi = 0°$ ($\phi = 180°$). The data points which (for experimental reasons, see text) have been excluded from the linear fits (full curves) are marked additionally by crosses. Included and excluded data points for $B_z = 41.8$ mT and $E_\perp \geqslant 200$ V/cm correspond to $\phi = 0°$ and $\phi = 180°$, respectively.

values scattering around 1.5, indicating a somewhat reduced number of states available for field mixing within the series of $Ni^{24+}(1s^2 2p_{3/2}nl)$ DR resonances. In calculations for Li-like Si^{11+} and C^{3+} ions, ratios of even less than 1 have been found [7,40]. This was attributed to the electrostatic quadrupole-quadrupole interaction between the $2p$ and nl Rydberg electron in the intermediate doubly excited state, which more effectively lifts the degeneracy between the $2p_{3/2}nl$ levels than between the $2_{1/2}nl$ levels. Another reason for the reduced number of $2p_{3/2}nl$ states participating in DRF might be the existence of additional Coster-Kronig decay channels for these resonances with $n \geqslant 20$ to $Ni^{25+}(1s^2 2p_{1/2})$ (cf. Sec. III A).

Slopes for the relative electric-field enhancement according to Eq. (16) were previously determined in measurements by Bartsch and co-workers for the lighter isoelectronic ions Si^{11+}, Cl^{14+}, and Ti^{19+} [12,8,10]. The present results are compared with these previous data in Fig. 11. It should be

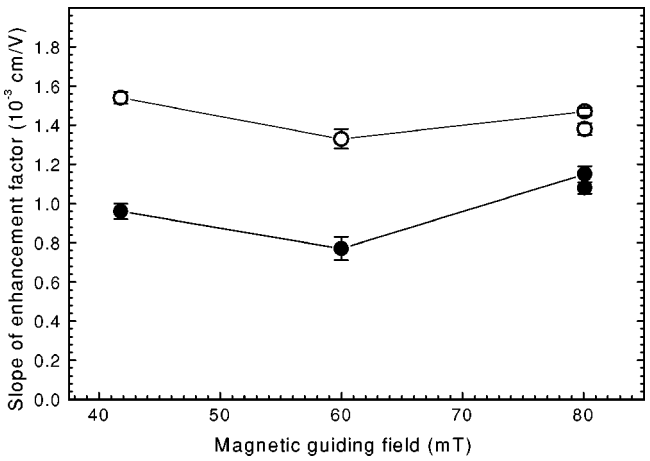

FIG. 10. Slopes of the enhancement factors as a function of the magnetic field B_z for the $2p_{3/2}nl$ (open symbols) and $2p_{1/2}nl$ (closed symbols) series of Rydberg resonances with $n \geqslant 31$.

noted that the comparison is only semiquantitative, because the choice of integration ranges for the calculation of the integrated recombination coefficients is somewhat arbitrary, and different cutoff quantum numbers n_{cut} exist for the different ions (cf. Table IV). Clearly, the relative enhancement for a given electric-field strength is much lower for Ni^{25+} than for the lighter ions studied so far, with the reduction for the step from lithiumlike titanium ($Z=22$) to nickel ($Z=28$), apparently much larger than the step from, e.g., chlorine ($Z=17$) to $Z=22$. As a general trend with increasing Z,

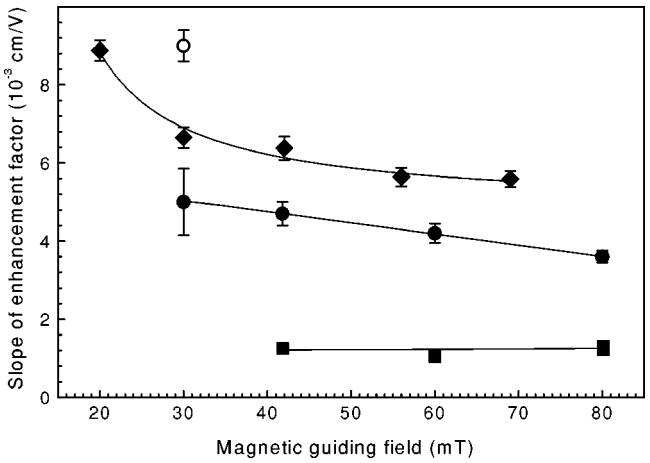

FIG. 11. Slopes of the enhancement factors as a function of the magnetic field B_z for the $2p_jnl$ resonances of Li-like Si^{11+} (open circle) [12], Cl^{14+} (diamonds) [8], Ti^{19+} (full circles) [10], and Ni^{25+} ions (squares) (this work). The lines are drawn to guide the eye. For Ti^{19+} and Ni^{25+}, where the field effects on the $2p_{1/2}$ and $2p_{3/2}$ series of DR resonances have been determined separately, the corresponding slopes have been averaged. Clearly the effects of external electric and magnetic fields on DR decrease with increasing nuclear charge. It should be noted that the Ti^{19+} slopes published in Ref. [10] are higher because they result from a nonlinear fit to the measured enhancement factors. For the comparison presented in this figure, a linear fit has been consistently applied for all ions under consideration.

TABLE IV. Parameters in DRF experiments with Li-like ions. For each ion the field effect has been quantified by considering an integrated DR rate coefficient which comprises the resonance strengths of $2p_jnl$ DR resonances with $n_{\min} \leqslant n \leqslant n_{\max}$, where $n_{\max}$ is the approximate cutoff quantum number due to field ionization in the charge-analyzing dipole magnet. It depends on the ion beam energy and the ion's charge state [30].

Ion	Reference	Ion beam energy (Mev/u)	$n_{\min}$		$n_{\max}$
			$2p_{1/2}$	$2p_{3/2}$	
Cl^{14+}	[8]	7.1	23	18	79
Ti^{19+}	[10]	4.6	27	27	115
Ni^{25+}	[this work]	5.9	31	31	150

the radiative decay rates A_r decrease $\propto Z$ for type-I transitions [see Eq. (11)] and $\propto (Z-3)^4$ for type-II transitions, while the autoionization rates are rather independent of Z. This shifts the range where the low-l autoionization rates are larger than the radiative stabilization rates (the condition for DR enhancement by l mixing to occur [5]) down to states of lower principal quantum number n for increasing Z. For Ni^{25+} the degree of mixing reached by the typical experimental field strengths appears to be much reduced as compared to lighter ions. In addition, a clear dependence of the electric field enhancement on the magnetic field strength is no longer observed for Ni^{25+}. To clarify the reason for the strong reduction of both the electric and additional magnetic-field effects in the heavy system studied here, detailed quantitative calculations are desirable.

External electric and magnetic fields are ubiquitous in astrophysical or fusion plasmas. Therefore, it is of interest to look into the implications of the field enhancement effect for the Ni^{25+} $\Delta n=0$ DR rate coefficient in a plasma. As an example, in Fig. 12 we show the ratio of rate coefficients derived from two measurements with and without an external electric field. As compared to zero electric field, the recombination coefficient at our highest experimental electric-

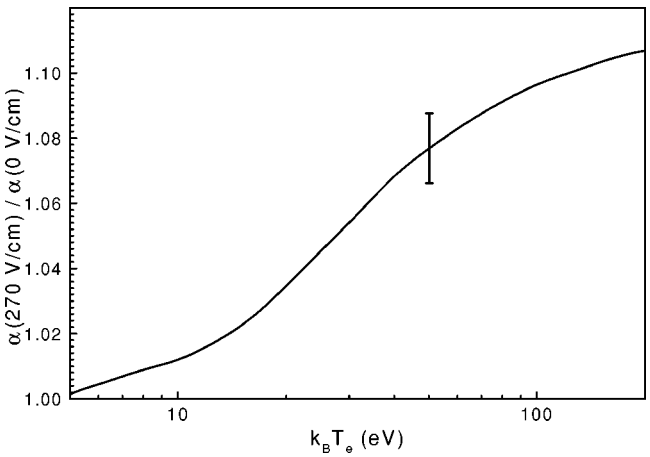

FIG. 12. Ratio of Ni^{25+} $\Delta n=0$ DR plasma rate coefficients with ($E_\perp = 270$ V/cm) and without ($E_\perp \approx 0$ V/cm) external electric field. The magnetic field was $B_z = 80$ mT. An experimental error bar of $\pm 1\%$, as indicated, is estimated for the ratio of the rate coefficient.

field strength ($E_\perp = 270$ V/cm at $B_z = 80$ mT) is enhanced by up to 11%. This value only represents a lower limit for the enhancement at the given field strength, as we observe DR resonances due to $Ni^{24+}(1s^2 2p_j nl)$ intermediate states only up to $n_{cut} \approx 150$. It should also be noted that in our experiments we did not reach an electric-field strength where the DR rate enhancement saturates.

IV. SUMMARY AND CONCLUSIONS

The recombination of lithiumlike Ni^{25+} ions has been experimentally studied in detail. Spectroscopic information on individual DR resonances associated with $Ni^{24+}(1s^2 2p_j nl)$ intermediate states, which have been experimentally resolved up to $n = 32$, has been extracted and the $\Delta n = 0$ DR plasma rate coefficient has been derived. Our experimental result is underestimated by up to a factor of 2 by semiempirically calculated rate coefficients. At plasma temperatures above 10 eV, results of detailed theoretical calculations are available [35] which agree well with the experiment. At lower temperatures, where Ni^{25+} ions may exist in photoionized plasmas, no data for the DR rate coefficient have been previously available.

In the presence of external electric fields up to 300 V/cm, the measured DR resonance strength is enhanced by a factor 1.5, a rather weak effect in comparison with previous measurements at $Z = 11$, 17, and 22. Due to the overall weakness of the field effect for Ni^{25+} ions, a marked dependence of the DR rate enhancement on the strength of a crossed magnetic field, as observed for Cl^{14+} and Ti^{19+} ions, has not been detectable in the present investigation.

Experimental limitations prevented us from obtaining an energy resolution in our DRF measurements comparable to that achieved in the field-free measurement. Consequently, we could not resolve a $Ni^{24+}(1s^2 2p_j nl)$ DR resonance with a value of n high enough to exhibit a field effect. Such an observation would have facilitated a direct comparison with *ab initio* calculations, which, due to the large number of nlm states to be considered, presently can only treat a single n manifold of Rydberg states in the presence of crossed $\vec{E}$ and $\vec{B}$ fields [7]. Improvements of this situation can be expected in the near future from the steady increase of computing power on the theoretical side, and on the experimental side from a dedicated electron target which is presently being installed at the TSR. With the electron target and the electron cooler operating at the same time, we will be able to perform DRF measurements with continuously cooled ion beams, yielding DRF spectra with increased resolution.

ACKNOWLEDGMENTS

We gratefully acknowledge support by the German Federal Ministry for Education and Research (BMBF) through Contract Nos. 06 GI 848 and 06 HD 854. R.P. acknowledges support from the Division of Chemical Sciences, U.S. Department of Energy, under Contract No. DE-FG03-97ER14787 with the University of Nevada, Reno.

[1] J. Dubau and S. Volonté, Rep. Prog. Phys. **43**, 199 (1980).
[2] A. Müller, in *Atomic and Plasma-Material Interaction Data for Fusion*, Nucl. Fusion Vol. 6 (IAEA, Vienna, 1995), pp. 59–100.
[3] B. W. Shore, Astrophys. J. **158**, 1205 (1969).
[4] Y. Hahn, Rep. Prog. Phys. **60**, 691 (1997).
[5] F. Robicheaux and M. S. Pindzola, Phys. Rev. Lett. **79**, 2237 (1997).
[6] F. Robicheaux, M. S. Pindzola, and D. C. Griffin, Phys. Rev. Lett. **80**, 1402 (1998).
[7] D. C. Griffin, F. Robicheaux, and M. S. Pindzola, Phys. Rev. A **57**, 2708 (1998).
[8] T. Bartsch, S. Schippers, A. Müller, C. Brandau, G. Gwinner, A. A. Saghiri, M. Beutelspacher, M. Grieser, D. Schwalm, A. Wolf, H. Danared, and G. H. Dunn, Phys. Rev. Lett. **82**, 3779 (1999).
[9] V. Klimenko, L. Ko, and T. F. Gallagher, Phys. Rev. Lett. **83**, 3808 (1999).
[10] T. Bartsch, S. Schippers, M. Beutelspacher, S. Böhm, M. Grieser, G. Gwinner, A. A. Saghiri, G. Saathoff, R. Schuch, D. Schwalm, A. Wolf, and A. Müller, J. Phys. B **33**, L453 (2000).
[11] S. Schippers, G. Gwinner, T. Bartsch, A. Hoffknecht, A. Müller, D. Schwalm, and A. Wolf, in *The Physics of Atomic and Electronic Collisions*, edited by Y. Itikawa *et al.*, AIP Conf. Proc. No. 500 (AIP, Melville, NY, 2000), p. 400.
[12] T. Bartsch, A. Müller, W. Spies, J. Linkemann, H. Danared, D. R. DeWitt, H. Gao, W. Zong, R. Schuch, A. Wolf, G. H. Dunn, M. S. Pindzola, and D. C. Griffin, Phys. Rev. Lett. **79**, 2233 (1997).
[13] A. Müller, D. S. Belić, B. D. DePaola, N. Djurić, G. H. Dunn, D. W. Mueller, and C. Timmer, Phys. Rev. Lett. **56**, 127 (1986); Phys. Rev. A **36**, 599 (1987).
[14] D. C. Griffin and M. S. Pindzola, Phys. Rev. A **35**, 2821 (1987).
[15] E. Jaeschke, D. Krämer, W. Arnold, G. Bisoffi, M. Blum, A. Friedrich, C. Geyer, M. Grieser, D. Habs, H. W. Heyng, B. Holzer, R. Ihde, M. Jung, K. Matl, R. Neumann, A. Noda, W. Ott, B. Povh, R. Repnow, F. Schmitt, M. Steck, and E. Steffens, in *Proceedings of the European Particle Accelerator Conference, Rome, 1988*, edited by S. Tazzari (World Scientific, Singapore, 1989), p. 365.
[16] A. Müller and A. Wolf, in *Accelerator-Based Atomic Physics Techniques and Applications*, edited by by J. C. Austin and S. M. Shafroth (AIP, New York, 1997), p. 147.
[17] A. Müller, Philos. Trans. R. Soc. London, Ser. A **357**, 1279 (1999).
[18] S. Schippers, Phys. Scr. **T80**, 158 (1999).
[19] A. Wolf, G. Gwinner, J. Linkemann, A. A. Saghiri, M. Schmitt, D. Schwalm, M. Grieser, M. Beutelspacher, T. Bartsch, C. Brandau, A. Hoffknecht, A. Müller, S. Schippers, O. Uwira, and D. W. Savin, Nucl. Instrum. Methods Phys. Res. A **441**, 183 (2000).

[20] G. Kilgus, D. Habs, D. Schwalm, A. Wolf, N. R. Badnell, and A. Müller, Phys. Rev. A **46**, 5730 (1992).
[21] A. Lampert, A. Wolf, D. Habs, J. Kenntner, G. Kilgus, D. Schwalm, M. S. Pindzola, and N. R. Badnell, Phys. Rev. A **53**, 1413 (1996).
[22] M. Grieser, M. Blum, D. Habs, R. V. Hahn, B. Hochadel, E. Jaeschke, C. M. Kleffner, M. Stampfer, M. Steck, and A. Noda, in *Cooler Rings and Their Applications*, edited by T. Katayama and A. Noda (World Scientific, Singapore, 1991), p. 190.
[23] S. Pastuszka, U. Schramm, M. Grieser, C. Broude, R. Grimm, D. Habs, J. Kenntner, H.-J. Miesner, T. Schüßler, D. Schwalm, and A. Wolf, Nucl. Instrum. Methods Phys. Res. A **369**, 11 (1996).
[24] B. Hochadel, F. Albrecht, M. Grieser, D. Habs, D. Schwalm, E. Szmola, and A. Wolf, Nucl. Instrum. Methods Phys. Res. A **343**, 401 (1994).
[25] G. Miersch, D. Habs, J. Kenntner, D. Schwalm, and A. Wolf, Nucl. Instrum. Methods Phys. Res. A **369**, 277 (1996).
[26] W. A. Huber and C. Bottcher, J. Phys. B **13**, L399 (1980).
[27] H. A. Bethe and E. E. Salpeter, *Quantum Mechanics of One- and Two-Electron Atoms* (Springer-Verlag, Berlin, 1957).
[28] L. H. Andersen and J. Bolko, Phys. Rev. A **42**, 1184 (1990).
[29] H. Hinnov, TFTR Operating Team, B. Denne, and JET Operating Team, Phys. Rev. A **40**, 4357 (1989).
[30] A. Müller and A. Wolf, Hyperfine Interact. **107**, 233 (1997).
[31] J.-G. Wang, T. Kato, and I. Murakami, Phys. Rev. A **60**, 2104 (1999).
[32] R. D. Cowan, *Theory of Atomic Structure and Spectra* (University of California Press, Berkeley, 1981).
[33] A. Burgess, Astrophys. J. **141**, 1588 (1965).
[34] R. Mewe, J. Schrijver, and J. Sylwester, Astron. Astrophys. **87**, 55 (1980).
[35] C. J. Romanik, Astrophys. J. **330**, 1022 (1988). An obvious misprint in the NiXXVI entry of Table 3 is $a_6 = 7.93 \times 10^{-9}$. It should read $a_6 = 7.93 \times 10^{-10}$. This value has been used to plot the curves in Fig. 5 of the present paper.
[36] H. Teng, B. Sheng, W. Zhang, and Z. Xu, Phys. Scr. **49**, 463 (1994).
[37] M. H. Chen, Phys. Rev. A **44**, 4215 (1991).
[38] D. W. Savin, T. Bartsch, M. H. Chen, S. M. Kahn, D. A. Liedahl, J. Linkemann, A. Müller, S. Schippers, M. Schmitt, D. Schwalm, and A. Wolf, Astrophys. J. Lett. **489**, L115 (1997).
[39] I. Nasser and Y. Hahn, Phys. Rev. A **36**, 4704 (1987).
[40] D. C. Griffin, D. Mitnik, M. S. Pindzola, and F. Robicheaux, Phys. Rev. A **58**, 4548 (1998).